Proprioceptivity and Upper-Extremity Dynamics in Robot-Assisted Reaching Movement

Marco Caimmi[1,2], Nicola Pedrocchi[1], Alessandro Scano[1],
Matteo Malosio[1], Federico Vicentini[1], Lorenzo Molinari Tosatti[1], Franco Molteni[2]

Abstract— **Reaching-against-gravity movements feature some remarkable aspects of human motion, like a wide exploration of the upper extremity workspace and high dynamics. In clinical rehabilitation protocols the recovery of the reaching movement capability is considered as a "paradigm" because of its fundamental role as a precursor for the use of the hand in activities of daily living. Reaching-based protocol may take advantage of robot usage, which has become a standard procedure in rehabilitation of neurological patients although the efficacy of the robot-assisted treatment is still matter of discussion. Even fewer studies in literature investigate proprioception, upper-extremity dynamics and their mutual relationship. Robot-assistance introduces alterations in the dynamics of movements, *e.g.* limited maximum velocities and accelerations, partial upper-extremity weight support, interaction forces between the robot and a subject. As a consequence, the subjects' proprioception may be altered too. The purpose of this preliminary work is to investigate the relationship between upper-extremity dynamics and proprioception by comparing the estimation of shoulder torques and EMG activation pattern with the evaluation given by the subjects on the quality of the perceived movements during different reaching trials with and without robot assistance. Results show that slow free (non-assisted) reaching movements are felt as uncomfortable and figure large shoulder torques and EMG cocontraction levels. Comfortable movements are those displaying shoulder torques and cocontraction levels comparable to those in natural free reaching, suggesting the strong correlation of torques patterns and co-contractions in motion comfort.**

I. Introduction

In the last fifteen-years many kinds of robots have been developed to assist the motion in the rehabilitation of neurologically impaired people [1]. Notwithstanding the high-technology level provided by current robotic devices, the debate on the efficacy of robot-assisted therapy is still open and no standards methods nor assistance modalities are universally recognized as unquestionably effective. At present, the mechanisms underlying the improvement in motor function following a robotic therapy are, in fact, not clear. The effect of interactions between subjects (both healthy and impaired) and the robots has not been deeply studied yet in the field of assistive robotics. This aspect is crucial because the subject's perception of motion is at the basis of the re-learning process at brain level. In the pioneeristic works of Sherrington the self-motion perception is often related to proprioception - "sensations elicited by stimulation of receptors within the body during subjects own movement" [2] - and, together with vision, proprioception operates in the planning and control of actions. As discussed in [3], although these sensations are thought to convey a variety of information, such as the force of a muscle contraction and the relative timing of motor commands [4], most of literature attention to date is paid to the ability of (self-)detecting positions and movements of body segments. Conversely, the dynamics of the upper-limb movements based on proprioceptive feedback has been largely ignored in the motor behavioral literature. Under-investigations of dynamics become therefore critical in robot-assisted rehabilitation where accelerations and joint torques are often largely affected by the interaction with the robot. Variations in robot dynamics (along programmed assistive motions) provide purposeful, still under-investigated, effects on subject-robot energy exchange. In addition, the effects of dynamic interaction undergo some joint torque alterations due to eventual operational conditions wherever (i) the weight of the upper-extremity (UE) is often partially supported and (ii) the movement velocities allowed in up to date robot-assisted training are usually slower than the physiological ones. The effects of reduced shoulder torques due to arm weight support on the subject's self-movement perception are unclear. Similarly, poor knowledge is devised about the increased shoulder torques due to the inefficient exchange of kinetic and potential energies in slow movements w.r.t. the physiological ones [5]. Summarizing, being clear that the interaction with the robot is of great impact on the self-movement perception, how such a mechanism takes place and which are the variables that play a primary role are still matter of study. The relevance of such features themselves and their consequences on the recovery process greatly require further investigation because the proprioceptive feedback is at the basis of the re-learning process [6].
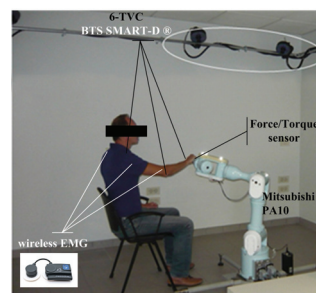

Fig. 1. Experimental setup: a 7-dof low-power industrial robot, a 3D tracking system, 6-channel free EMG devices, a 6-axes force/torque sensor.

[1] with Institute of Industrial Technology and Automation, CNR, 20133 Milan, Italy `marco.caimmi@itia.cnr.it`
[2] with Hospital Valduce - Villa Beretta, via Nazario Sauro 17, 23845 Costa Masnaga, Italy.
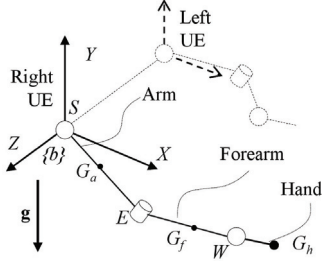
Fig. 2. UE model with 4 dof, *i.e.*, pronosupination is neglected andnd the hand is reproduced as a fixed appendage mass of the forearm.

As a consequence, the aim of the present work is twofold. First, to analyse the effects of the interaction with robot on the UE dynamics of subjects performing various robot-assisted reaching movements against gravity[1] in different robot control modalities and levels (e.g. power) of interaction (see Fig. 1). Second, to investigate whether and how the self-motion perception during either free or robot-assisted reaching against gravity is related to shoulder joint torques and shoulder muscles EMG activation patterns. Such study purposes are addressed introducing the UE dynamics solution and the underlying limb model in section II. Self-movement perception and corresponding dynamics are evaluated according to some trials whose methods and the results are in section III. Critical issues are discussed in section IV.

II. BIOMECHANICAL MODEL OF THE UPPER EXTREMITY

According to the purposes of the study, some assumptions are introduced:

i. the model is used to describe only the reaching against gravity, *i.e.* not pursuing general purpose modeling;
ii. hand is modelled a lumped mass displaying translations;
iii. the position of the shoulder center of rotation is considered fixed, *i.e.* the arm and forearm inertia forces due to shoulder translation are neglected[2] as in [7].

Under these assumptions, the kinematics and dynamics of the UE movement may be modeled as a serial chain with 7 degrees-of-freedom. Several UE models are available in literature for the kinematic analysis, while dynamics is usually modeled considering the whole limb as a serial actuated chain of rigid links, providing very straightforward interface for standard multi-body engines [8], [9], [10]. Nevertheless, human articular joints are just coarsely simplified as serial actuated axes, being more accurately similar to parallel kinematic mechanisms. Being the analysis of joints, specifically shoulder torques, the main purpose of the model, the computation of dynamics is simplified according to the following notation. All figures are expressed in a global coordinate frame $\{b\}$ centered on the shoulder whose axes are aligned with principal body planes, *i.e.* displaying X (anterior/posterior), Z (left/right), and Y (upwards/downwards).

[1]Reaching against gravity is paradigmatic for ADL training.
[2]The single trial is immediately repeated in case the subject does not fulfills the instructions to keep trunk and head steady

As detailed in Fig. 2, the centers of rotation of the articular joints shoulder S, elbow E and wrist W are denoted as

$$S \equiv [x_s\, y_s\, z_s]^T_{\{b\}}, \ E \equiv [x_e\, y_e\, z_e]^T_{\{b\}}, \ W \equiv [x_w\, y_w\, z_w]^T_{\{b\}} \quad (1)$$

and G_a, G_f, G_h are the centers of mass of the arm, the forearm and the hand, respectively. Finally, let $\mathbf{u}_a \equiv \mathbf{u}_a\,(E, S)$, $\mathbf{u}_f \equiv \mathbf{u}_f\,(W, E)$, and $\mathbf{u}_h \equiv \mathbf{u}_h\,(G_h, W)$ be the unit vectors relative to the arm, forearm and hand axis, computed as:

$$\mathbf{u}_a = \frac{E - S}{\|E - S\|}, \quad \mathbf{u}_f = \frac{W - E}{\|W - E\|}, \quad \mathbf{u}_h = \frac{G_h - W}{\|G_h - W\|}. \quad (2)$$

Under the reported assumption of a purely translating hand, the direction of the vector from its center of mass to the wrist is always parallel to axis X. Denoting as $\mathbf{e}_x$ the unit vector of axis X, the hand axis constraint is expressed as $\mathbf{u}_h \cdot \mathbf{e}_x \equiv 0$.

A. First Order Kinematics

Denote as $\boldsymbol{\omega}_a$ and $\boldsymbol{\omega}_f$ the angular velocity of the arm and forearm respectively. According to the angular velocity physical meaning, $\boldsymbol{\omega}_f$ and $\boldsymbol{\omega}_a$ may be split into two terms:

$$\boldsymbol{\omega}_f = \boldsymbol{\omega}_f^\perp + \boldsymbol{\omega}_f^\parallel \quad \text{and} \quad \boldsymbol{\omega}_a = \boldsymbol{\omega}_a^\perp + \boldsymbol{\omega}_a^\parallel$$

$$\text{such that} \begin{cases} \boldsymbol{\omega}_f^\perp \cdot \mathbf{u}_f = 0 \\ \boldsymbol{\omega}_f^\parallel \times \mathbf{u}_f = 0 \end{cases} \text{and} \begin{cases} \boldsymbol{\omega}_a^\perp \cdot \mathbf{u}_a = 0 \\ \boldsymbol{\omega}_a^\parallel \times \mathbf{u}_a = 0. \end{cases} \quad (3)$$

Terms $\boldsymbol{\omega}_f^\parallel$ and $\boldsymbol{\omega}_a^\parallel$ represent the rotation of the body segments around their own axis. Under assupmtions (i) and (ii), pronosupination is negligible, $\boldsymbol{\omega}_f^\parallel \simeq \mathbf{0}$ and $\boldsymbol{\omega}_f \simeq \boldsymbol{\omega}_f^\perp$. As the intra/extra rotation $\boldsymbol{\omega}_f^\perp$ is imposed directly from the rotation around the arm axis $\mathbf{u}_a$, the following equation yields:

$$\boldsymbol{\omega}_a^\parallel = \left(\boldsymbol{\omega}_f^\perp \cdot \mathbf{u}_a\right)\mathbf{u}_a. \quad (4)$$

Angular velocities may be computing from joints position using the following fundamental mechanics relationships:

$$\boldsymbol{\omega}_f^\perp \times \mathbf{u}_f = \frac{d}{dt}\mathbf{u}_f \quad \text{and} \quad \boldsymbol{\omega}_a^\perp \times \mathbf{u}_a = \frac{d}{dt}\mathbf{u}_a. \quad (5)$$

Due to the orthogonality condition imposed by (3), the angular velocities are finally expressed as:

$$\boldsymbol{\omega}_f \simeq \boldsymbol{\omega}_f^\perp = \mathbf{u}_f \times \frac{d}{dt}\mathbf{u}_f$$

$$\boldsymbol{\omega}_a = \mathbf{u}_a \times \frac{d}{dt}\mathbf{u}_a + \left(\mathbf{u}_f \times \frac{d}{dt}\mathbf{u}_f \cdot \mathbf{u}_a\right)\mathbf{u}_a. \quad (6)$$

B. Dynamics

Let be m_a, l_a (m_f, l_f, m_h, l_h) the mass and length of the arm (forearm and hand) and consider two additional hypotheses: (i) the arm may be modeled as a rod of constant section made of homogeneous material; (ii) the inertial term around the arm axis is negligible. The angular momentums of the arm, the forearm and the hand w.r.t. the shoulder S may be expressed as:

$$\mathbf{L}_a^S = \frac{1}{3}m_a\, l_a^2\, \boldsymbol{\omega}_a^\perp,$$

$$\mathbf{L}_f^S = m_f\,(G_f - S) \times \frac{d}{dt}(G_f - S) + \frac{1}{12}m_f\, l_f^2\, \boldsymbol{\omega}_f^\perp, \quad (7)$$

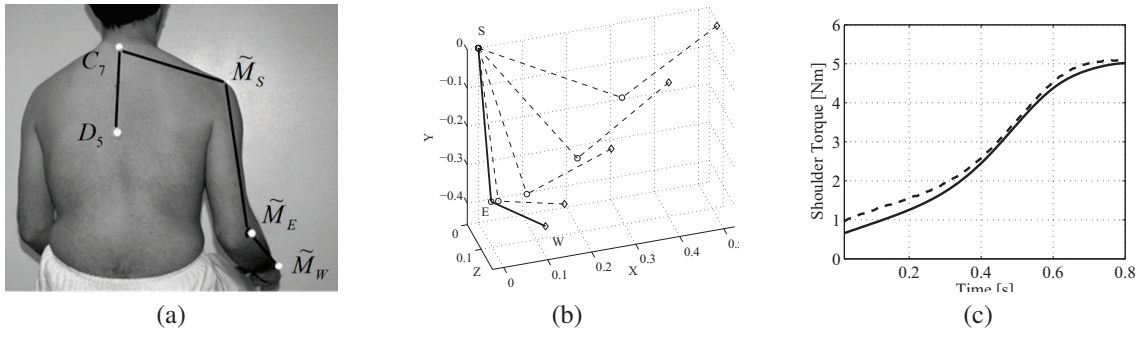$$\mathbf{L}_h^S = m_h\,(G_h - S) \times \frac{d}{dt}(G_h - S)$$

Fig. 3. markers approximation validation: (a) markers position for UE tracking; (b) simulation of reaching trajectory in is biomimetic and calculated from filtering real acquired ones; (c) shoulder flexo-estension torque projected along XY plane: the torque is computed using nominal articular joints S, E, W (solid line) or noisy markers positions $\widetilde{M}_S$, $\widetilde{M}_E$, $\widetilde{M}_W$ measuring the corresponding articular joints centers (dashed line).

respectively. Let $\mathbf{F}_{ext}$ be the external forces on the wrist that, being the subject's hand constrained to the robot handle (see Fig. 1), are sampled with the force sensor. Denoting as $\mathbf{g}$ the gravity, the shoulder torque $\mathbf{T}_s$ can be computed as:

$$
\begin{aligned}
\mathbf{T}_s = & \frac{d}{dt}\Big[\mathbf{L}_a^S + \mathbf{L}_f^S + \mathbf{L}_h^S\Big] \\
& - \Big[m_a\,(G_a - S) + m_f\,(G_f - S) + m_h\,(G_h - S)\Big] \times \mathbf{g} \\
& - \mathbf{F}_{ext} \times (W - S)\,.
\end{aligned} \tag{8}
$$

C. Articular Centers Estimation

A passive marker infra-red cameras system has been used for the kinematic acquisition. Among the most common sources of uncertainty, skin artefacts and a large variability in anthropometric parameters hinder the accuracy of the estimation of the articular centers [11], [12]. A correspondingly common procedural approach involves the use of a large number of markers, although different protocols making use of very few markers [13] allow a good estimation of the UE kinematic as well. In the present study, the adopted protocol makes use of 5 hemispherical retroreflective markers [5] applied on the spinous process of D5, the spinous process of C7, the acromion $\widetilde{M}_S$, the lateral epicondyle of the elbow $\widetilde{M}_E$, and the styloid process of the ulna $\widetilde{M}_W$ (see Fig. 3-(a)). As in [13], with this procedure the measured position of markers placed onto the shoulder, the elbow and the wrist, respectively, can be reasonably assumed as their corresponding articular joints centers S, E, W, i.e. $S \approx \widetilde{M}_S$, $E \approx \widetilde{M}_E$, $W \approx \widetilde{M}_W$. Fig. 3-(c) displays the results of two dynamic simulations of the model described in (8) obtained by kinematics computation using either nominal joints centers (e.g. S) and noisy corresponding markers positions (e.g. $\widetilde{M}_S$), along nominal realistic trajectories (see Fig. 3-(b)). The approximation introduced by this protocol is considered acceptable for the purpose of the present analysis.

III. Torque Analysis on Reaching Movements

A. Materials & Methods

Nomenclature: *path* is the curve in the Cartesian space; *motion law* is the evolution over time of the curvilinear coordinate along the path; *trajectory* is defined as a path with an associated law of motion; *natural path* and *natural*
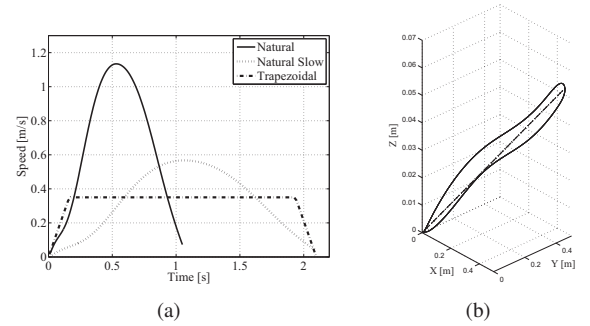

Fig. 4. Trajectories: (a) *natural* (solid), *slow natural* (dotted) and *constant* (dashed) velocity ; (b) *natural* (solid) and *straight* (dashed) paths.

velocity are the path and the velocity corresponding to the non-assisted reaching performed at a self-selected speed; *natural slow velocity* corresponds to a motion law scaling the natural velocity by a factor of two; *constant velocity* is a motion law with constant acceleration/deceleration (see Fig. 4-(a)); *straight path* is a *path* with start and end points coincident to the ones of the *natural path* (see Fig. 4-(b)); *follow strategy* means that subject is asked to move grasping robot handle and trying to follow its movement minimizing the interaction forces; *push strategy* means that each subject is asked to move grasping the robot handle and trying to slightly anticipate its movement; *active strategy* means that the robot is constrained to the *path*, and the subject is asked to move the robot handle along the *path* by pushing the robot. **Robot setup** includes a controller that allows to record and execute complex *paths* and *motion laws* (see Fig. 5). *Paths* are described as 3D analytical splines (the subject's hand and the robot end effector display pure translations). *Motion laws* can be independently assigned to each path by associating a velocity profile to the curvilinear coordinates. *Paths* and *motion laws* can be loaded into the control loop either by processing the camera tracking system data or by directly recording the position of the robot handle when manually driven by the operator. Robot and cameras coordinate frames are calibrated according to the procedure in [14]. In addition, the control allows the execution of hybrid trajectories constraining the robot handle along a given path and letting the motion law to be imposed by the subject (see mode (A)

Fig. 5) according to an admittance model.

Participants: Six healthy subjects (29±5 years, 1 female).
Equipment: An end-effector based robot (Mitsubishi Pa10-7), a 6 TVC 3D-motion tracking system coupled with wireless EMG (BTS Smart D with FreeEMG), a Force/Torque sensor at the robot handle and a safety inertial device attached to the fifth robot link.
Study Design: Subjects were requested to perform 12 consecutive reaching movements against gravity, first in natural (non-assisted) conditions [5], then in interaction with the robot. The *natural paths* with and *natural velocities* have been tracked during the natural movement, then averaged and scaled to the same starting and ending positions and the movement average duration doubled. Each subject therefore performed a total of 12 trials derived by combinations of path pairs (straight/natural) and velocities pairs (constant/natural). Trials trajectories were implemented by the robot in order to provide the subjects with assisted movements. Each trial will be indicated as **T-k** hereafter, where **k** is the progressive index of the trial. Table I reports the correspondence between the trial and the typology of exercise.
Dependent measures: (i) a 5 point Visual Analogue Scale (VAS) about how natural and comfortable the movement was felt (see I); (ii) the cocontraction level (percentage) between deltoid anterior and deltoid posterior muscles; (iii) the elevation shoulder torque (see section II-B).

B. Results

Tab.I reports both the VAS score assigned to different trials and the cocontraction levels of anterior/posterior deltoids.
General remarks about the VAS score. A default score 5 is assigned to non-assisted reaching movements performed at *natural velocity*, which acts as reference value for comfortable feeling. Then, (i) the **T-1** is the worst perceived, with the almost lowest score of 3.5 points; (ii) all movements with *natural slow velocity* are felt comfortable (scored ≥ 4); (iii) movements with *constant velocity* are felt uncomfortable (scored averagely 3.5); (iv) path type seems to have low influence on VAS in case of fully assisted movements while remarkably difference emerged in partial assisted movement; (v) the *follow/push* interaction modes happen to be irrelevant for the assignment of VAS scores. Compared to **T-0**, all other movements but the ones partially assisted, present statistically significant differences. All other inter-trials differences are not statistically significant.
General remarks about the cocontraction levels. A reference value of 34% in anterior/posterior deltoids cocontraction level is observed in **T-0**. Then, (i) **T-1** presents the largest cocontraction level (44%); (ii) all robot-assisted movements display cocontraction levels equal to or lower than **T-1**; (iii) cocontraction values almost equal to the **T-1** are observed in all movements requested to *follow* the robot, while reduced cocontraction w.r.t. **T-1** are referable to all trials where the subject was asked to actively *push* the robot; (iv) *natural paths* seem to induce low cocontraction levels; (v) velocities profiles display negligible influence on the cocontraction level. Observation (i) is confirmed by statistical analysis

($p < .03$) while (iii-iv) are trends not confirmed by the statistics. Nevertheless, all robot-assisted movements present no statistically significant differences in cocontraction levels w.r.t. the reference movement.
General remarks about the shoulder torque. The analysis of shoulder torque $\mathbf{T}_s$ is limited to the elevation moment T_s, that is, denoting as $\mathbf{e}_z$ the unit vector of axis Z, $T_s = \mathbf{T}_s \cdot \mathbf{e}_z$. Different trials T_s patterns are displayed in Figs. 6, 7 and 8. T_s is made of two components, a gravity and an inertia terms. In case of movements performed at *natural velocity* (see Fig. 6-(a)), T_s smoothly increases until a maximum in correspondence of the acceleration peak. Subsequently, T_s remains approximately steady around 75% of the gravity term maximum, henceforth denoted as T_s^{75}. When the subject is forced to perform the movement at lower speed (Fig. 6-(b)), the T_s profile almost resembles the pattern of the gravity term. In particular, during the deceleration phase no limitations on T_s occur so that the 100% of the torque due to the limb weight is reached. In Fig. 7, the T_s of each trial is compared with T_s of the two non-assisted reaching movements (**T-0** and **T-1**). Considering the trials on the left column of figures array (*follow* mode), T_s^{75} happens to be reached about at 50% of the movement or slightly earlier. In case of robot end-effector *constant velocity* (**T-2** and **7**) the T_s increase displays a small linear rate, regardless the kind of path, resembling the pattern typical of slow movements. In case of *natural slow velocity* profiles (**T-4** and **9**), the T_s increase rate is larger at the beginning of the movement before settling in between the patterns of *natural* and *slow* movements. This is evident for the *natural path* where T_s^{75} is reached in about 30% of the movement duration. Along all these four trials T_s is basically constant and equal to T_s^{75} in the second part of the movement. Considering instead the trials on the right column (*push* mode), the T_s increase rate significantly exceed that of **T-0**, up to a maximum of almost twice T_s^{75}. In **T-5** and **8** (*natural slow velocity*), the T_s maximum is slightly lower than in **T-3** and **10** (*constant velocity*); the timing of T_s^{75} crossing is also different, *i.e.* around 50% and 25% of movement duration, respectively. The second part of the movement seems to be influenced by both the path and the velocity profile. Although in all movements T_s decreases down to T_s^{75}, before remaining basically constant until the end of the movement, the timing is different for all **T-3**, **5**, **8** and **10**, occurring at 70%, 90%, 80% and 100%, respectively. Considering **T-6** and **11**, where the robot handle is driven by the subject, the T_s rate and maximum value are higher than those of all other trials. Differences between **T-6** and **11** are negligible.

C. Discussion

The aims of this work have been specifically posed to (i) study the effect robot interaction on the upper-extremity dynamics during reaching against gravity movements and to (ii) investigate the possible correlation between a subject's self-motion perception and the shoulder elevation torques T_s and EMG cocontraction levels. Considering that during robotic treatment the maximum velocities are generally
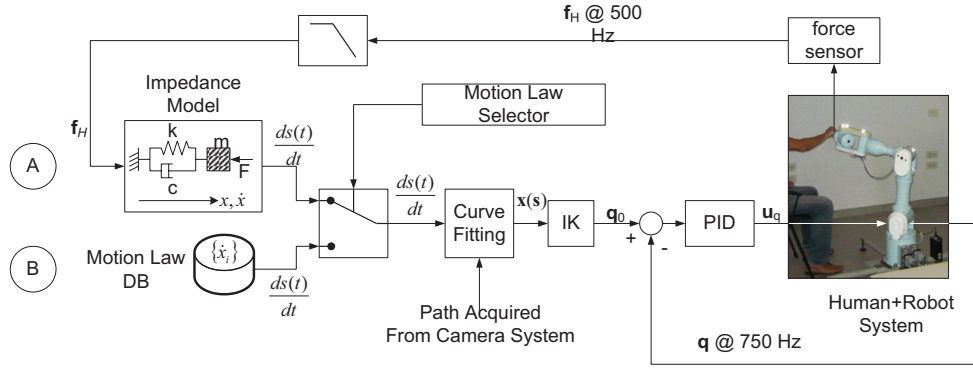
Fig. 5. Robot control architecture implementing different training modes: along a path loaded from a previous acquisition with the tracking system, the motion law results from an admittance model imposed by external forces (A) or loaded from a database (B). Interaction forces are low-pass filtered from the end-effector force sensor.

TABLE I
EXPERIMENT RESULTS

| | | Free Mov. | | Complete Assistance | | | | Partial Assistance |
| | | | | Follow | | Push | | |
				Natural Vel.	Constant Vel.	Natural Vel.	Constant Vel.	
TRIALS CODE [-]	Straight Path	-	-	**T-4**	**T-2**	**T-5**	**T-3**	**T-6**
	Natural Path	**T-0**	**T-1**	**T-7**	**T-9**	**T-10**	**T-8**	**T-11**
VAS [-]	Straight Path	x	x	4.3	3.4	4.6	3.3	3.7
	Natural Path	5	3.5	4.1	3.6	4.0	3.6	4.5
AD/PD cocontraction* [%]	Straight Path	-	-	34 ± 10	34 ± 7	33 ± 9	29 ± 10	32 ± 14
	Natural Path	34 ± 6	44 ± 6	33 ± 8	33 ± 4	28 ± 8	28 ± 8	33 ± 9

*Anterior deltoid (AD) vs posterior deltoid (PD) cocontraction calculated as in [15]. Cocontraction is computed from 0% to 50% of the forward movement, that is the acceleration phase of the movement. Analysis is limited to this time-window because (i) healthy subjects have few time to adapt themselves to the exercise and (ii) it corresponds to the phase where subjects exert positive work while the deceleration phase is characterized by energy dissipation.

TABLE II
WILCOXON TEXT (AD/PD COCONTRACTION)

	T-0	T-1	T-2	T-3	T-4	T-5	T-6	T-7	T-8	T-9	T-10	T-11
T-0	-	$p < 0.03$	n.s.	n.s.	n.s.	n.s.	n.s.	n.s.	n.s.	n.s.	n.s.	n.s.
T-1	$p < 0.03$	-	$p < 0.03$	$p < 0.03$	n.s.	$p < 0.03$	n.s.	$p < 0.04$	$p < 0.03$	$p < 0.03$	$p < 0.03$	$p < 0.03$

(a) **T-0** (natural path, natural velocity)

(b) **T-1** (natural path, natural slow velocity)
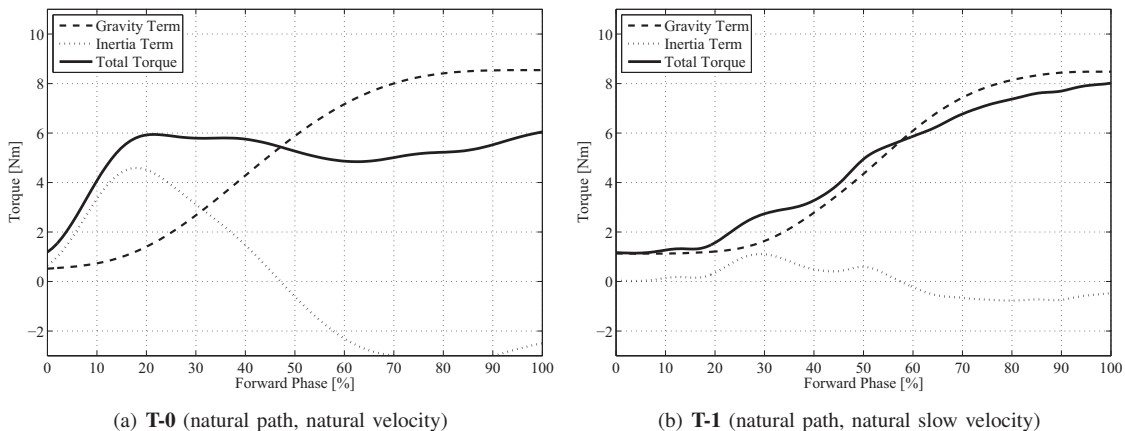
Fig. 6. Torque at Shoulder of one subject for not assisted movements

(a) **T-2** (straight path, natural slow velocity, follow)

(b) **T-3** (straight path, natural slow velocity, push)

(c) **T-4** (straight path, constant velocity, follow)

(d) **T-5** (straight path, constant velocity, push)

(e) **T-7** (natural path, constant velocity, follow)

(f) **T-8** (natural path, constant velocity, push)

(g) **T-9** (natural path, natural slow velocity, follow)

(h) **T-10** (natural path, natural slow velocity, push)
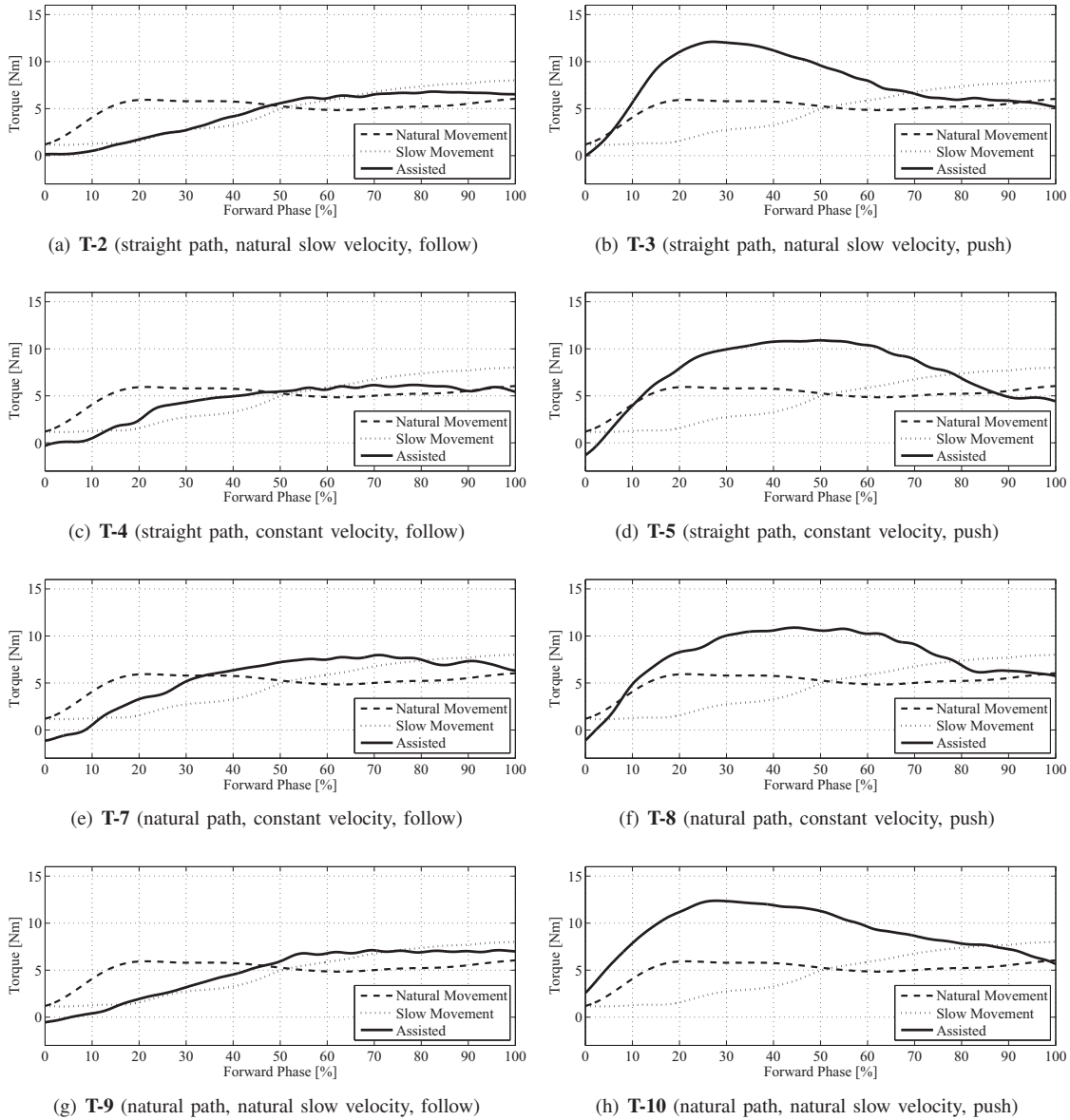
Fig. 7.   Shoulder torque T_s of one subject for assisted movements.

(a) **T-6** (straight path, active)

(b) **T-11** (natural path, active)
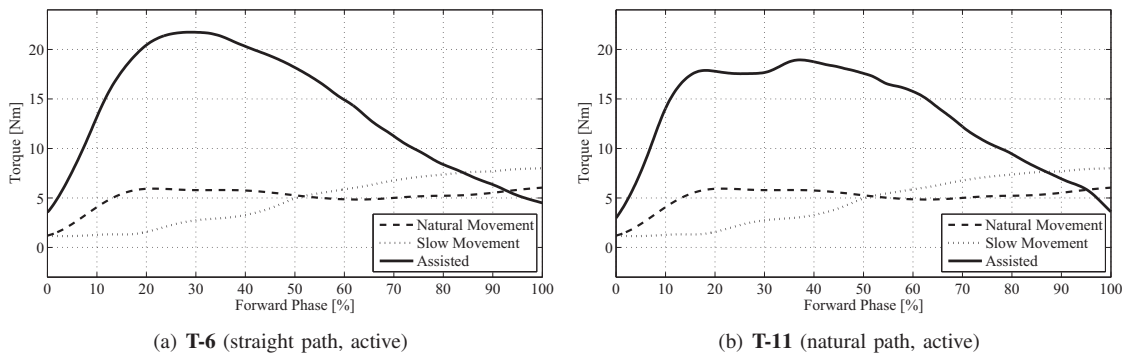
Fig. 8.   Shoulder torque T_s of one subject for partially assisted movements.

limited, experimental comparisons about the UE dynamics took into consideration a set of movements performed at both low and self-selected speed. The latter is characterized by a smooth interchange of kinetic and potential energies and, consequently, T_s at the end of movements is limited to around 75% of the torque due to the limb weight. Contrarily, during slow movements, the kinetic energy is limited and a movement may be considered to be quasi-isometric. In this situation the deltoid posterior is activated for stabilizing the limb and, consequently, the cocontraction level increases. As a result, the movement is more fatiguing due to two main reasons: (i) the required torque is higher and (ii) the exerted torque is inefficiently applied during the movement. These are probably the reasons underlying the assignment of a very low VAS score to **T-1**. Surprisingly, the previously described increase in the T_s at final stage of the movement is, in all robot-assisted trials, perfectly compensated by the decrease in required torque due to the weight support given by the robot. Likely, it seems that a subject with a normally functioning motor control is able to automatically adapt and balance the joint torque reproducing the original natural movement pattern, notwithstanding the completely different dynamics of the performed movement. The level of cocontraction, in fact, regains the physiological value and extra energy expenditure no longer occurs. Such an hypothesis is generally confirmed by the fact that the robot-assisted movements scored higher than **T-1**. The weight support, which could potentially be perceived as a troublesome constraint and have a negative effect on the self-motion perception, probably counterbalance the side effects of low/limited velocities. Encouragingly, the robot assistance turns out to be a medium for the recovery of the natural proprioception.

VAS results also report the subjects sensitivity about velocity profiles that, in turn, seem to be correlated to the T_s shape, particularly during the acceleration phase. Preferred natural velocity profiles, instead, do not correlate with the cocontraction levels. This is barely surprising because (i) velocities (and accelerations) are very low and (ii) cocontractions are already limited by the weight support that makes additional stabilization of the limb unnecessary. From the energy perspective, low cocontraction levels are correlated to the *push* modality, for performing which the anterior deltoid activity increases to supply the requested extra torque (higher rate of T_s increase). This torque demand involves physiological mechanisms of inhibition of the antagonist muscle. The *push* modality as well as the **T-6** and **11**, for which a subject is requested to actively drive the robot handle, are, in fact, felt comfortable by tested subjects.

IV. CONCLUSIONS

As a pilot study for clinical trials dedicated to reaching recovery in neurological patients, this work has investigated the dynamics of the human-robot interaction in eligible movements. Reaching movements are, in fact, selected because of their importance in daily living and because are anti-gravity patterns. The use of an assistive robot in this class of movements significantly modifies the subject' pro-

prioception, because UE weight is partially supported by the robot that, in turn, completely alter the ballistic nature of the movement. The present work investigated the relationship between the UE-robot coupled dynamics and proprioception by comparing the shoulder torques and EMG activation patterns with an evaluation given by the subjects' about the quality of the perceived movements. Results show that slow non-assisted reaching movements are felt uncomfortable due to large shoulder torques and high EMG co-contraction levels. Arguably, no correlation between VAS and EMG in robot-assisted movements can be established, while, interestingly, it seems that a strong correlation holds between the shoulder torque profile and the personal perception of the motion. Finally, experiments display that T_s profile is more related to the *motion law* imposed by the robot than to the followed *path*. Robot trajectories-related results are, quite surprisingly, mirrored by personal perception,*i.e.* the VAS scores.

REFERENCES

[1] Y. Hayashi and K. Kiguchi, "A lower-limb power-assist robot with perception-assist," in *Rehab. Rob., Proc. of IEEE Int. Conf. on*, 29 June 2011-July 1 2011, pp. 1–6.

[2] C. Sherrington, "On the proprio-ceptive system, especially in its reflex aspects," *Brain*, vol. 29(4), pp. 467–482, 1907.

[3] M. A. Buckley, A. Yardley, G. R. Johnson, and D. A. Cams, "Dynamics of the upper limb during performance of the tasks of everyday living: A review of the current knowledge base," *Proc. of the Instit. of Mech.l Eng.: J.l of Eng. in Medicine*, vol. 210(4), pp. 241–247, 1996.

[4] W. Ferrell and B. Craske, "Contribution of joint and muscle afferents to position sense at the human proximal interphalangeal joint," *Experimental Physiology*, vol. 77(2), pp. 331–342, 1992.

[5] M. Caimmi, S. Carda, C. Giovanzana, E. S. Maini, A. M. Sabatini, N. Smania, and F. Molteni, "Using kinematic analysis to evaluate constraint-induced movement therapy in chronic stroke patients." *Neurorehab.ilitation and Neural Repair*, vol. 22(1), pp. 31–39, 2008.

[6] D. M. Wolpert, R. C. Miall, and M. Kawato, "Internal models in the cerebellum," *Trends in Cognitive Sciences*, vol. 2(9), pp. 338–347, 1998.

[7] E. Pennestrí, R. Stefanelli, P. Valentini, and L. Vita, "Virtual musculo-skeletal model for the biomechanical analysis of the upper limb," *J. of Biomechanics*, vol. 40(6), pp. 1350–1361, 2007.

[8] S. Delp, F. Anderson, A. Arnold, P. Loan, A. Habib, C. John, E. Guendelman, and D. Thelen, "Opensim: Open-source software to create and analyze dynamic simulations of movement," *Biomedical Engineering, IEEE Tran. on*, vol. 54(11), pp. 1940 –1950, nov. 2007.

[9] J. Rosen, J. Perry, N. Manning, S. Burns, and B. Hannaford, "The human arm kinematics and dynamics during daily activities - toward a 7 dof upper limb powered exoskeleton," in *Advanced Robotics, 2005. ICAR '05. Proc.., 12th Int. Conf. on*, july 2005, pp. 532 –539.

[10] E. Rocon, A. Ruiz, J. Pons, J. Belda-Lois, and J. Sanchez-Lacuesta, "Rehabilitation robotics: a wearable exo-skeleton for tremor assessment and suppression," in *Robotics and Automation, Proc. of the IEEE Int. Conf. on*, april 2005, pp. 2271 – 2276.

[11] M. A. Nussbaum and X. Zhang, "Heuristics for locating upper extremity joint centres from a reduced set of surface markers," *Human Movement Science*, vol. 19(5), pp. 797–816, 2000.

[12] T.-W. Lu and J. O'Connor, "Bone position estimation from skin marker coordinates using global optimisation with joint constraints," *J. of Biomechanics*, vol. 32(2), pp. 129–134, 1999.

[13] O. Rettig, L. Fradet, P. Kasten, P. Raiss, and S. I. Wolf, "A new kinematic model of the upper extremity based on functional joint parameter determination for shoulder and elbow," *Gait and Posture*, vol. 30(4), pp. 469–476, 2009.

[14] F. Vicentini, N. Pedrocchi, M. Malosio, and L. Molinari Tosatti, "High-accuracy hand-eye calibration from motion on manifolds," in *Intelligent Robots and Systems, PRoc. of IEEE/RSJ Int. Conf. on*, sept. 2011, pp. 3327–3334.

[15] D. A. Winter, "Calculation and interpretation of mechanical energy of movement," *Exercise and Sport Sciences Reviews*, vol. 6, pp. 183–201, 1978.